

# Combinatorial substrate epitaxy investigation of polytypic growth of $AEMnO_3$ ( $AE = Ca, Sr$ )

Catherine Zhou<sup>1</sup>  | Marc De Graef<sup>1</sup> | Bogdan Dabrowski<sup>2</sup> | Gregory S. Rohrer<sup>1</sup>  | Paul A. Salvador<sup>1</sup> 

<sup>1</sup>Department of Materials Science and Engineering, Carnegie Mellon University, Pittsburgh, PA, USA

<sup>2</sup>Institute of Physics, Polish Academy of Sciences, Warsaw, Poland

## Correspondence

Paul A. Salvador, Department of Materials Science and Engineering, Carnegie Mellon University, 5000 Forbes Ave., Pittsburgh, PA 15213, USA.

Email: paulsalvador@cmu.edu

## Funding information

National Science Foundation, Grant/Award Number: DMR-1609355; US Department of Defense Vannevar-Bush Faculty Fellowship, Grant/Award Number: N00014-16-1-2821; Carnegie Mellon University, Grant/Award Number: MCF-677785

## Abstract

Combinatorial substrate epitaxy (CSE) was used to study the orientation relationships (ORs) and polytypic stability of  $AEMnO_3$  ( $AE = Ca, Sr$ ) thin films grown on polycrystalline  $SrMnO_3$  and  $SrTiO_3$  substrates.  $SrMnO_3$  films with the stable four-layered hexagonal ( $4H$ ) and metastable three-layered cubic ( $3C$ ) structures were also grown on (111) and (100)  $SrTiO_3$  single crystal substrates, respectively. Electron backscatter diffraction data were used to determine the following ORs, which hold true regardless of the substrate surface orientation:  $(001)[100]_{4H SrMnO_3} || (001)[100]_{4H SrMnO_3}$ ,  $(111)[\bar{1}\bar{1}0]_{3C CaMnO_3} || (001)[100]_{4H SrMnO_3}$ , and  $(001)[100]_{4H SrMnO_3} || (111)[\bar{1}\bar{1}0]_{3C SrTiO_3}$ . These are all simply the eutactic OR, which aligns the eutactic planes and directions; its ubiquity indicates that the interface energy is generally lower for the eutactic OR than for all other possible ORs.  $3C SrMnO_3$  was found to grow only on very near (100)  $3C SrTiO_3$  grains. This narrow range of epitaxial stabilization suggests that the penalties of higher interfacial and/or strain energies between polytypic perovskites adopting the eutactic OR are not significant enough to overcome the volumetric formation energy of the stable phase in these growth conditions, except for very special orientations.

## KEYWORDS

characterization, interfaces, orientation relationships, thin films

## 1 | INTRODUCTION

Epitaxial stabilization is a method known to direct growth of a specific compound as a film in a particular crystal structure, using a supporting substrate as the template.<sup>1–3</sup> Importantly, it has been used to grow metastable phases where other synthesis methods have failed.<sup>2,4–11</sup> When optimized for epitaxial stabilization, nucleation of a bulk metastable phase is thermodynamically preferred due to a lower free energy of formation for its epitaxial nuclei,<sup>2,3</sup> with important contributions from the film-substrate interface and strain energies. Most epitaxy studies use commercially available single crystal substrates with polished, low Miller index surfaces and high

planar symmetries. These experiments are therefore limited to a small number of structural, strain, orientation, and symmetry states of surfaces, usually those representing special interfaces of a limited number of structural types. Therefore, our understanding of epitaxy and our ability to stabilize polymorphs across wide ranges of structures is hindered by the lack of available commercial isostructural substrates across wide-ranging orientations.

Combinatorial substrate epitaxy (CSE) is a high-throughput method to investigate epitaxial growth that overcomes the limitations of traditional epitaxy investigations. In CSE, polished polycrystalline substrates are used, which can be prepared in-house for a wide range of structural families, and

each grain of the substrate can be viewed as a single crystal with a unique orientation. Electron backscatter diffraction (EBSD) is used in CSE as a high-throughput local structural probe to create phase and orientation maps across large areas of the substrate surface, as well as the deposited film.<sup>8–15</sup> A single deposition of a film onto a polycrystalline substrate yields thousands of observations from which a broad understanding of phase stability and film-substrate orientation relationships (ORs) can be developed. For example, only a few ORs were found for epitaxial films on polycrystalline substrates across all of orientation space of the substrate.<sup>9,11,12</sup> One common preferred epitaxial orientation (PEO) is called the eutactic OR, which aligns the eutactic (or nearly close-packed) planes and directions between the film and substrate.<sup>9,11,12</sup> Furthermore, CSE has been used many times now to investigate polymorph stability, including anatase vs rutile TiO<sub>2</sub><sup>8,9</sup> and rutile vs scrutinyite SnO<sub>2</sub>.<sup>11</sup> Based on these prior observations, we use CSE herein to epitaxially grow SrMnO<sub>3</sub> and CaMnO<sub>3</sub> perovskite polytype thin films on both cubic and hexagonal polycrystalline perovskite substrates, investigating epitaxial stabilization and preferred orientation relationships.

Alkaline-earth (AE) manganese oxide perovskites, AEMnO<sub>3</sub> (AE = Ca, Sr, and Ba), are of special interest because they can form over the full range of perovskite polytypes and exhibit varying physical properties.<sup>16–24</sup> These polytypes differ in the relative number or order of cubic and hexagonal stacking of the eutactic AEO<sub>3</sub> planes, which leads to variations in the number of corner-shared or face-shared MnO<sub>6</sub> octahedra.<sup>17,23,25,26</sup> Because many of the physical properties of manganese oxide perovskites are associated with details of the Mn–O bonding, controlling the polytype formation is critical to engineering properties as a function of composition.<sup>18,27,28</sup> The primary approach used to control polytype formation is to control the Goldschmidt tolerance factor,  $t$ ,<sup>29</sup> which describes the relative similarity between the AE–O and Mn–O bond lengths (more information about  $t$  can be found in Appendix S1). Under normal processing conditions, BaMnO<sub>3</sub> ( $t \approx 1.06$ <sup>17</sup>) forms the 2H structure with all face-sharing octahedra and a stacking sequence ABAB; SrMnO<sub>3</sub> ( $t \approx 0.99$ <sup>17</sup>) forms the four-layered hexagonal (4H) structure with half face-sharing and half corner-sharing octahedra and a stacking sequence ABCB; and CaMnO<sub>3</sub> ( $t \approx 0.94$ <sup>17</sup>) forms an orthorhombic variant of the 3C polytype with all corner-sharing octahedra and a stacking sequence ABC.<sup>30–32</sup> Importantly, the polytype formed for a given cation composition depends on temperature, pressure, and oxygen activity.<sup>24</sup> At temperatures above 1400°C, for example, SrMnO<sub>3</sub> evolves sufficient oxygen that the 4H structure transforms to 3C.<sup>31</sup> Interestingly, Song et al.<sup>19</sup> determined the influences of oxygen pressure and temperature on the phase stability of SrMnO<sub>3</sub> thin films, using (111) 3C SrTiO<sub>3</sub> substrates, which were similar to those for bulk material. While

CaMnO<sub>3</sub> and BaMnO<sub>3</sub> form in different variants or polytypes of their respective structures at elevated temperatures,<sup>30,33</sup> neither have been formed with complete hexagonal or cubic stacking, respectively.

It is of interest to develop synthetic methods that would allow access to distinct polytypes independent of composition and tolerance factor, which would thus open up observation of new materials, such as ferroelectric and ferromagnetic 3C BaMnO<sub>3</sub>.<sup>34</sup> Epitaxial stabilization has been used to grow 3C SrMnO<sub>3</sub> films on single crystal {100} 3C perovskite substrates,<sup>19,35–37</sup> in conditions that the 4H polytype is known to be stable as a thin film on (111) 3C SrTiO<sub>3</sub>. These observations support the ideas that epitaxial stabilization offers an independent parameter to influence polytype stability and that the observed epitaxial polytype will be a strong function of substrate orientation. However, very little is known for perovskite polytype epitaxy across orientation space on hetero-polytypic substrates, especially on 4H substrates, as they are not available in single crystal forms. While one can envision specific substrates will serve as strong drivers for stabilizing metastable polymorphs, there is no clear understanding the competitive nucleation events occurring during perovskite polymorph formation as epitaxial films.

Herein, we have carried out CSE experiments in which AEMnO<sub>3</sub> (AE = Ca, Sr) films were deposited on 4H SrMnO<sub>3</sub> and 3C SrTiO<sub>3</sub> polycrystalline substrates, as well as (100) and (111) 3C SrTiO<sub>3</sub> single crystals. We test whether the eutactic OR is the PEO for SrMnO<sub>3</sub> films deposited on 3C SrTiO<sub>3</sub> and 4H SrMnO<sub>3</sub> polycrystalline substrates, as well as CaMnO<sub>3</sub> films on 4H SrMnO<sub>3</sub> substrates. We find that the eutactic OR is the PEO for all film-substrate combinations, indicating the eutactic OR results in low energy interface relative to all other possible ORs. We also investigate phase stability of SrMnO<sub>3</sub> on SrTiO<sub>3</sub> over the entire range of substrate orientations, finding a surprisingly narrow range of orientations that stabilize 3C films in growth conditions for which 4H SrMnO<sub>3</sub> are stable.<sup>19</sup> We discuss these observations in the context of the interface energies for the epitaxial films and how they may influence perovskite polytype stability.

## 2 | EXPERIMENTAL DETAILS

Polycrystalline 3C SrTiO<sub>3</sub> (preparation described elsewhere<sup>12</sup>), 3C CaMnO<sub>3</sub>, and 4H SrMnO<sub>3</sub> ceramics were prepared using standard ceramic methods as targets and/or substrates. For 3C CaMnO<sub>3</sub> and 4H SrMnO<sub>3</sub> substrates, stoichiometric amounts of CaCO<sub>3</sub> or SrCO<sub>3</sub> and MnO<sub>2</sub> were mixed in ethanol, then ball-milled wet for 12 hours, and subsequently pressed uniaxially in a stainless-steel die at pressures >10000 psi. Samples were fired in air at 700°C, 1000°C, and 1350°C for 2, 24, and 24 hours, respectively. Prior to the second and third heating steps, samples were reground dry,

a portion used to monitor phase progression (using X-ray diffraction), and the rest pressed again for firing. Substrate (target) pellets were  $\approx 0.5$  (5) mm thick and 12 (25) mm in diameter. Sintered substrates were polished to a mirror finish using SiC paper and  $\text{Al}_2\text{O}_3$  suspensions. Additionally,  $5 \times 5 \times 0.5 \text{ mm}^3$ , one-side polished single crystals of (111) and (100)  $\text{SrTiO}_3$  were purchased from MTI Corporation.

All films were grown using a pulsed laser deposition (PLD) system<sup>8–10,12</sup> and a KrF ( $\lambda = 248 \text{ nm}$ ) laser. Prior to deposition, substrates were ultrasonically cleaned in methanol and ethanol for 10 minutes each, dried with compressed air, and attached to the substrate heater with silver paint. The chamber was pumped to base pressures around  $10^{-5}$  torr. Substrates were heated to  $850^\circ\text{C}$  at  $10^\circ\text{C}/\text{min}$ . The laser energy density was maintained at  $\approx 1.5 \text{ J}/\text{cm}^2$  and the target-to-substrate distance at  $\approx 6 \text{ cm}$ . Target surfaces were laser conditioned first at the base pressure for 10 000 and 2000 pulses, at 4 and 3 Hz, respectively. Then, the  $\text{O}_2$  pressure was brought up to the deposition pressure of 2 mTorr and target surfaces were laser conditioned for 2000 pulses at 3 Hz and at  $850^\circ\text{C}$ . Films were deposited for 6,000 pulses to obtain a thickness of  $\approx 60 \text{ nm}$ , based on a deposition rate of  $\approx 0.1 \text{ \AA}/\text{pulse}$ . The deposition rate was determined using X-ray reflectivity of  $\text{AEMnO}_3$  films grown on (111)  $\text{MgO}$ , using 6000 pulses at  $850^\circ\text{C}$  and 2 mTorr. Films were cooled at a rate of  $10^\circ\text{C}/\text{min}$  in 200 Torr  $\text{O}_2$ .

Phase and orientation for substrates and films were determined using EBSD in a Quanta 200 scanning electron microscope (SEM), as described elsewhere.<sup>11</sup> Identical areas were mapped on the substrate and the films, respectively, before and after deposition. EBSD patterns from the substrates were sharp and readily indexed using default settings in the Orientation Imaging Microscopy (OIM) Analysis software by EDAX. Film patterns were more diffuse, as reported elsewhere<sup>11</sup> from internal strain, and automated indexing was optimized by manual selection of reflectors used by OIM. An alternative indexing method, called dictionary indexing, is implemented in Appendix S5. EBSD patterns were indexed using cubic symmetry  $3C$  structures (the small orthorhombic distortions in  $\text{CaMnO}_3$  were ignored, which improved the confidence index (CI) in OIM) and hexagonal symmetry  $4H$  structures. All raw orientation maps were processed using

a minimum grain size of  $5 \mu\text{m}$  and a grain tolerance angle of  $5^\circ$ . ORs were extracted from the EBSD data as described elsewhere.<sup>9</sup>  $\text{SrMnO}_3$  films were also deposited on single crystals of (111) and (100)  $\text{SrTiO}_3$ , and their structures were characterized using XRD and EBSD.

### 3 | RESULTS

Deposition on  $3C$   $\text{SrTiO}_3$  single crystals was used to establish growth conditions for epitaxy and phase competition that are similar to literature observations. The XRD patterns of 60-nm  $\text{SrMnO}_3$  films deposited (at  $850^\circ\text{C}$  and 2 mTorr  $\text{O}_2$ ) on (111) and (100)  $3C$   $\text{SrTiO}_3$  single crystal substrates are shown in Figure 1A and B, respectively. Film peaks on both crystal substrates appear as reported in the literature<sup>19,35,36</sup> for epitaxial growth of  $\text{SrMnO}_3$ , indicating the growth conditions should be appropriate for CSE.

In Figure 1A, the highest intensity peaks belong to the (111) and (222) reflections of the (111)  $3C$   $\text{SrTiO}_3$  substrate ( $2\theta = 39.9^\circ$  and  $86.2^\circ$ ), while the two smaller peaks are attributed to the (002) and (006) reflections ( $2\theta = 19.6^\circ$  and  $61.4^\circ$ ) of  $4H$   $\text{SrMnO}_3$ . This indicates that the stable polymorph forms on this orientation of  $\text{SrTiO}_3$  in these deposition conditions, as expected.<sup>19</sup> The  $c$ -axis lattice parameter computed from these values is  $\approx 9.04 \text{ \AA}$ , which differs by 0.2% from the bulk  $4H$   $\text{SrMnO}_3$   $c$ -axis measured by Chamberland et al.<sup>23</sup>

In Figure 1B, the (100), (200), and (300) reflections from the (100)  $3C$   $\text{SrTiO}_3$  substrate correspond to the high intensity peaks at  $2\theta = 22.7^\circ$ ,  $46.4^\circ$ , and  $72.5^\circ$ , respectively. The lower intensity peaks at  $2\theta = 23.4^\circ$  and  $48.0^\circ$  correspond respectively to the (100) and (200) reflections of  $3C$   $\text{SrMnO}_3$ , although the peaks are shifted to larger  $2\theta$  values by  $\approx 0.6^\circ$  to  $1.3^\circ$  compared those expected for relaxed, stoichiometric  $3C$   $\text{SrMnO}_3$ . The out-of-plane lattice parameter computed for the  $3C$  film is  $3.80 \text{ \AA}$ , which is smaller (by  $-0.3\%$ ) than the bulk value of  $3.81 \text{ \AA}$ .<sup>38</sup> This is consistent with either in-plane tensile and out-of-plane compressive strains from epitaxial mismatch with the cubic substrate ( $3.905 \text{ \AA}$ ) or compositional deviations that lead to a change in lattice parameter along one or two directions of the pseudo-cubic cell, with a short

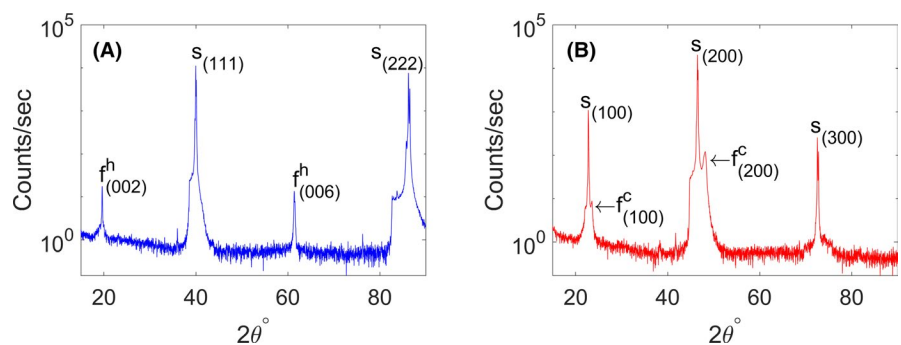


**FIGURE 1** XRD patterns of (A) a  $4H$   $\text{SrMnO}_3$  thin film grown on (111)  $\text{SrTiO}_3$  and (B) a  $3C$   $\text{SrMnO}_3$  film grown on (100)  $\text{SrTiO}_3$ .  $f^i$  ( $s$ ) indicates film (substrate) peaks of phase  $i = h$  (hexagonal) or  $c$  (cubic). The subscripts give the Miller indices of each peak [Color figure can be viewed at [wileyonlinelibrary.com](http://wileyonlinelibrary.com)]

(long) axis out-of-plane (in-plane) for a preferred epitaxial match.<sup>36,39,40</sup> We did not further differentiate these possibilities. This pattern indicates that the metastable polymorph forms on this orientation of  $3C$  SrTiO<sub>3</sub> in these deposition conditions, as expected.<sup>35–37</sup> Since the films in Figure 1 were deposited simultaneously, the polytype of SrMnO<sub>3</sub> films is a function of substrate orientation.

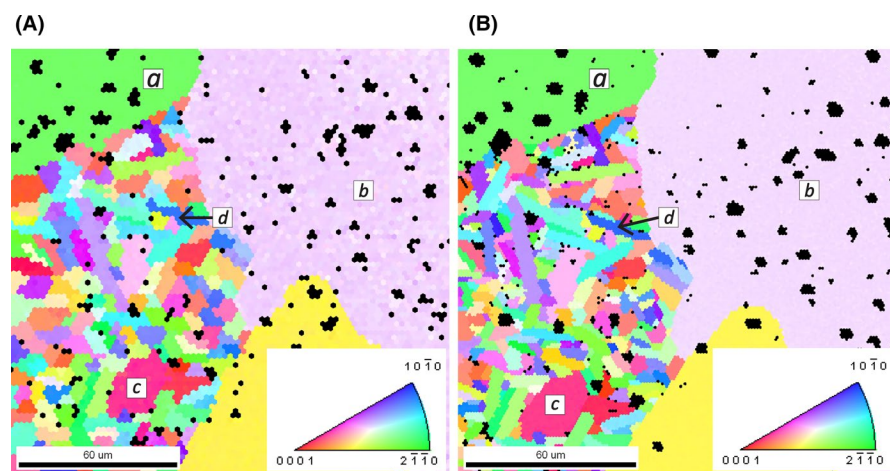
Orientation maps were constructed using EBSD data to further confirm the phase and epitaxial orientation of SrMnO<sub>3</sub> films on SrTiO<sub>3</sub> single crystal substrates (results shown in Appendix S2). Using XRD data in conjunction with EBSD data, the epitaxial relationships for the  $4H$  and  $3C$  SrMnO<sub>3</sub> films deposited on (111) and (100)  $3C$  SrTiO<sub>3</sub> substrates, respectively, were determined. The  $4H$  film on the  $3C$  substrate ( $f$ - $s$ ) has the epitaxial relationship:  $(001)[100]_{4H-f} || (111)[1\bar{1}0]_{3C-s}$ , which is the eutaxial OR. The  $3C$  film on the  $3C$  substrate has a unit-cell over unit-cell epitaxial OR:  $(100)[1\bar{1}0]_{3C-f} || (100)[1\bar{1}0]_{3C-s}$ , which is also consistent with the eutaxial OR.

Orientation maps of a  $4H$  SrMnO<sub>3</sub> substrate and  $4H$  SrMnO<sub>3</sub> film deposited on the same region are shown in Figure 2. The entire film was indexed as  $4H$  SrMnO<sub>3</sub> (the phase map is shown in Appendix S3), even when the OIM software considered the  $3C$  phase as a possibility. A minimum image quality (IQ) was set to remove erroneous orientations related to physical holes on the surface of the substrate or film, which are colored black. The average CIs for phase and orientation assignment given in Figure 2A and B were 0.50 and 0.39, respectively. Note that between substrate and film maps (as with others shown later), there is a slight rotation due to remounting of the sample inside of the chamber. However, the film grew in a grain-over-grain fashion, as the number, shapes, and colors of grains are similar in both images, as seen in grains labeled  $a$ – $d$ . It should also be noted that a smaller step size was used during EBSD pattern acquisition in Figure 2B compared to that of Figure 2A.

Figure 3 shows the orientation maps for the deposition of  $3C$  CaMnO<sub>3</sub> on a  $4H$  SrMnO<sub>3</sub> substrate. The phase map

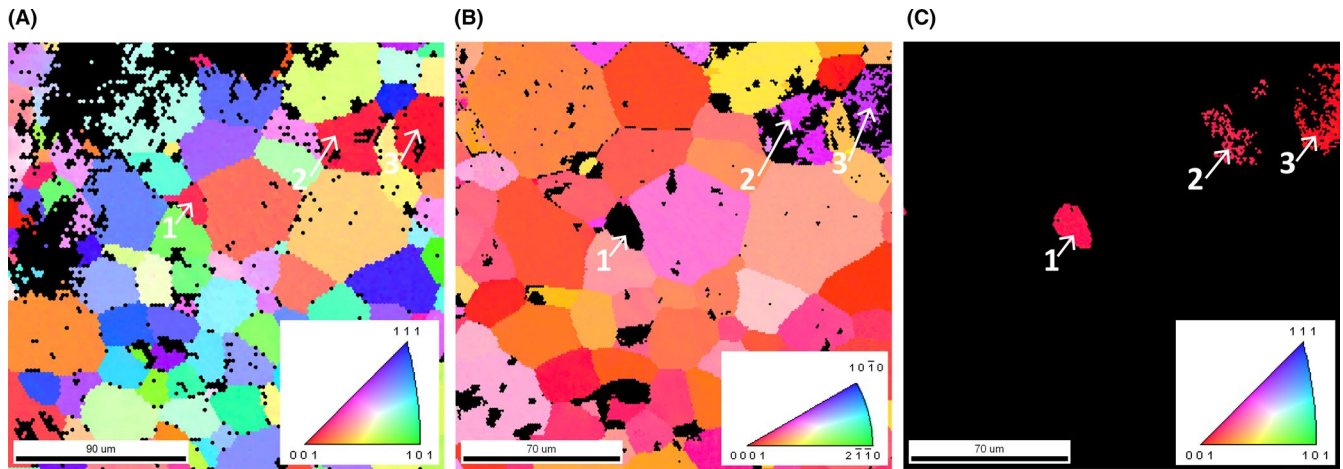
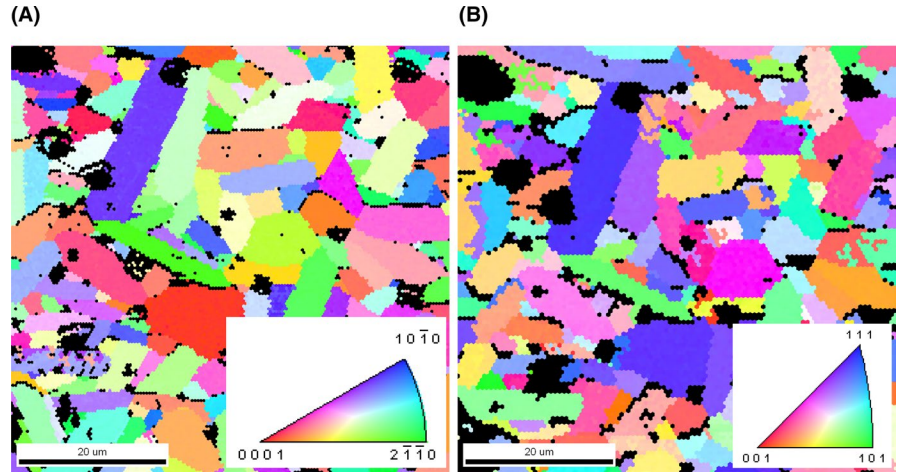
shown in Appendix S3 indicates that the CaMnO<sub>3</sub> film was almost entirely  $3C$ . Thus, only the  $3C$  CaMnO<sub>3</sub> partition is shown in the orientation map of Figure 3B. The average CI for the substrate and film in Figure 3A and B was 0.40 and 0.19, respectively. Despite the polytype difference between film and substrate, the growth again appears as grain-over-grain growth, as the number and shapes of grains are similar in both images. The colors in each image represent different orientations, and similarity/differences in color require further interpretation using the OR analysis discussed later.

Figure 4 shows the orientation maps of the SrMnO<sub>3</sub> film on a  $3C$  SrTiO<sub>3</sub> substrate. The phase map is shown in Appendix S3. The CI of the  $3C$  SrTiO<sub>3</sub> substrate in Figure 4A was 0.41, which is similar to those from the single crystal substrates discussed in Appendix S2. Furthermore, these CIs are similar to the  $4H$  SrMnO<sub>3</sub> substrates, indicating that OIM is relatively confident in determining grain orientations using a single  $3C$  or  $4H$  phase. The average CI for the  $4H$  SrMnO<sub>3</sub> film partition (Figure 4B) was 0.34, which is slightly lower than those described above for  $4H$  films and substrates, but still reasonable for a thin film. The average CI for the  $3C$  SrMnO<sub>3</sub> partition (Figure 4C) was 0.21, which is higher than that of the film on a (100)  $3C$  SrTiO<sub>3</sub> and similar to the previous  $3C$  CaMnO<sub>3</sub> film. As for both previous CSE cases, the SrMnO<sub>3</sub> film grew largely in a grain-over-grain fashion. While the majority of the film indexed as the stable  $4H$  polytype in Figure 4B, several distinct regions indexed as the metastable  $3C$  SrMnO<sub>3</sub> polytype, shown in Figure 4C. The  $4H$  film grains in Figure 4B are mostly red/orange to mauve/yellow in color, in contrast to the full color range observed for the films on the  $3C$  substrate. This indicates that the  $4H$  structure tends to grow in a limited region near the (001) orientation of hexagonal orientation space, despite the substrate exhibiting all orientations across the cubic orientation space. This observation is similar to the CSE growth of hexagonal Fe<sub>2</sub>O<sub>3</sub> on SrTiO<sub>3</sub>,<sup>12</sup> owing to the eutaxial OR governing the CSE growth.



**FIGURE 2** Orientation maps of (A) a  $4H$  SrMnO<sub>3</sub> substrate with (B) a  $4H$  SrMnO<sub>3</sub> film deposited on the same region

**FIGURE 3** Orientation maps of (A) a  $4H$   $\text{SrMnO}_3$  substrate with (B) a  $3C$   $\text{CaMnO}_3$  film deposited on the same region



**FIGURE 4** Orientation map of (A) a polycrystalline  $3C$   $\text{SrTiO}_3$  substrate with (B) the  $4H$   $\text{SrMnO}_3$  film grains partition and (C) the  $3C$   $\text{SrMnO}_3$  film grains partition

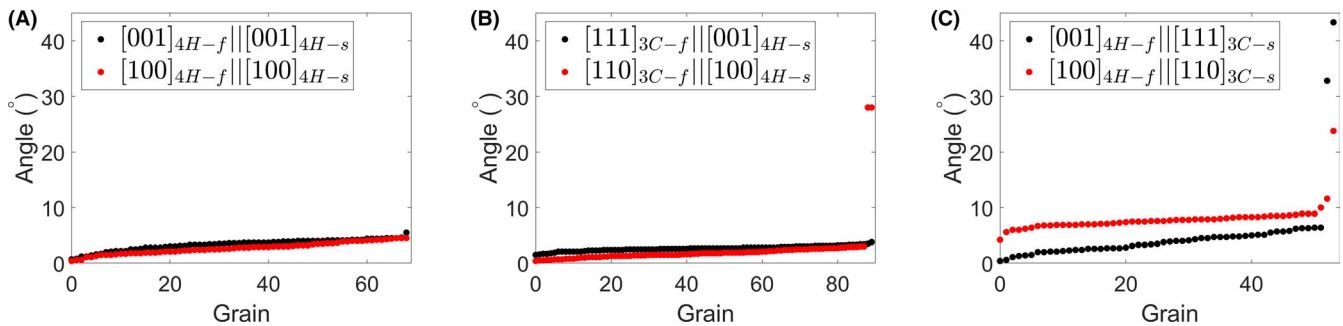


**FIGURE 5** Angle between (A)  $4H$   $\text{SrMnO}_3$  film on  $4H$   $\text{SrMnO}_3$  polycrystalline substrate from Figure 2, (B)  $3C$   $\text{CaMnO}_3$  film on  $4H$   $\text{SrMnO}_3$  polycrystalline substrate from Figure 3, and (C)  $4H$   $\text{SrMnO}_3$  film on  $3C$   $\text{SrTiO}_3$  polycrystalline substrate from Figure 4. Black dots represent the angles between the normals of the eutactic planes of film and substrate. Red dots represent the angles between directions in the eutactic planes.  $f$  stands for film and  $s$  stands for substrate

The  $3C$   $\text{SrMnO}_3$  partition shown in Figure 4C shows that areas of  $3C$  growth were (100) oriented and correlated to substrate grains that are near (100), similar to results from single crystal experiments above. Examples include grains marked as 1, 2, and 3. Grain 1 is an example of grain-over-grain

growth of metastable  $3C$   $\text{SrMnO}_3$  on  $3C$   $\text{SrTiO}_3$ . Grains 2 and 3 were indexed as near (100)  $3C$   $\text{SrMnO}_3$  and near (0334)  $4H$   $\text{SrMnO}_3$ , while the substrate grains were also near (100)  $3C$   $\text{SrTiO}_3$ . The Kikuchi patterns that indexed as having different polytypes throughout grains 2 and 3 looked mostly

identical within each grain, although some patterns had missing bands. As a result, OIM had difficulty assigning the local phase and orientation in these grains. Compared to other CSE investigations for metastable film growth,<sup>9,11,12,14</sup> the angular region of 3C epitaxial stabilization is narrower than reported for other metastable phases, but the preference for an individual orientation stabilizing metastable polymorphs is similar.

ORs between substrate and film grains were analyzed for all three CSE experiments using OIM data and our in-house program that determines the angle between specific crystallographic vectors in the film and substrate. The distribution of orientations for all substrates and films are shown in their respective stereographic triangles in Appendix S4. An assessment of the eutaxial OR is plotted in Figure 5, as the angles between the normals to the eutactic planes and the angle between eutactic directions lying in the eutactic planes. In Figure 5, the grains have been ordered by increasing angular differences between planar normals.

For the homoepitaxial deposition of 4H SrMnO<sub>3</sub> on the 4H SrMnO<sub>3</sub> substrate, 69 substrate-film pairs were recorded. All grain orientations in the 4H SrMnO<sub>3</sub> film correspond to a similar orientation of the 4H substrate (see grains *a* – *d* in Figure 2), with the exception of a few points, leading to a similar distribution of points in orientation space (see Appendix S4). The average angle between the normals of the eutactic (001) planes is 3.3° with a standard deviation of 1.0°, while the average angle between the in-plane direction, [100], is 2.7° with a standard deviation of 1.0°. The average difference between these angles, ≈3°, arises primarily from an uncertainty in remounting the sample in the SEM chamber. The standard deviation arises from uncertainty in the absolute assignment of orientations, grain averaging during processing, and local variations from relaxation during film growth. These values support that these homoepitaxial films adopt the eutaxial OR, which here corresponds to the alignment of hexagonal unit-cells, as expected. This OR can be written as (001)[100]<sub>4H-f</sub>|||(001)[100]<sub>4H-s</sub>.

For the deposition of 3C CaMnO<sub>3</sub> on the 4H SrMnO<sub>3</sub> substrate, 90 substrate-film pairs were recorded. Substrate and film grain orientations were evenly distributed across orientation space (see Appendix S4), although the corresponding indices are different owing to the different crystal systems. From the data shown in Figure 5B, the average angle between the normal to the eutactic planes, (001) for 4H and (111) for 3C, is 2.6° with a standard deviation of 0.4°, while the average angle between the eutactic directions within the planes, [100] for 4H and [110] for 3C, is 1.8° with a standard deviation of 0.7°, ignoring two outliers. The two outliers had an in-plane rotation of 28° and were not examined any further. These values support the assertion that the epitaxial OR is the eutaxial OR, regardless of substrate orientation, for 3C CaMnO<sub>3</sub> film on a 4H SrMnO<sub>3</sub> substrate (observed for 98% of grains). This OR can be written as: (111)[110]<sub>3C-f</sub>|||(001)[100]<sub>4H-s</sub>.

For the deposition of SrMnO<sub>3</sub> on the 3C SrTiO<sub>3</sub>, 54 substrate-film pairs were identified for 4H SrMnO<sub>3</sub> grains, and 3 substrate-film pairs for those corresponding to 3C SrMnO<sub>3</sub> grains (grains partially indexed as 4H and 3C were included in both distributions, for example, grains 2 and 3 in Figure 4). The substrate grains are distributed across orientation space, while the 4H and 3C grains (see Appendix S4) are clustered around the (001) for both phases. From the data shown in Figure 5C, the average angle between eutactic plane normals for the 4H film and 3C substrate is 3.7°, with a standard deviation of 1.6° (ignoring the outliers) while the average angle between the in-plane eutactic directions is 7.6°, with a standard deviation of 1.1° (again ignoring outliers). The latter value is relatively large, and is likely related to relaxations occurring for this heteroepitaxial system. These values support that the epitaxial OR is the eutaxial OR for a 4H SrMnO<sub>3</sub> film on 3C SrTiO<sub>3</sub>. This can be written as: (001)[100]<sub>4H-f</sub>|||(111)[110]<sub>3C-s</sub>. For the three 3C grains, the unit-cell over unit-cell, eutaxial OR is observed.

## 4 | DISCUSSION

Using CSE, we have analyzed the polytypic epitaxial growth of 3C and 4H perovskites on 3C and 4H substrates. As observed for other CSE experiments,<sup>8–15</sup> our films exhibited grain-over-grain epitaxy, allowing each individual grain to be treated as a single crystal, even for orientations with high Miller indices. All of the data shown above supports the hypothesis that the eutactic OR is the PEO for AEMnO<sub>3</sub> films on 4H SrMnO<sub>3</sub> and 3C SrTiO<sub>3</sub> polycrystalline substrates, over all of orientation space (ignoring the few outliers). We then observed that the range of orientations of 3C SrTiO<sub>3</sub> that stabilized the metastable 3C SrMnO<sub>3</sub> phase was very narrow and close to (100) in these growth conditions, which were similar to those investigated previously using single crystals. There were no significant observations of metastable 4H CaMnO<sub>3</sub> film grains on 4H SrMnO<sub>3</sub> polycrystalline substrates. Overall, these observations shed light onto polytype epitaxy and epitaxial stabilization in the perovskite system, described below.

The observations reported here support the utility of CSE as a high-throughput approach to establishing general PEOs for different film-substrate structural pairs under specific epitaxial growth conditions. The existence of a single OR (the eutactic OR) over all of orientation space for all film-substrate pairs also supports the assertion that growth, or computational modeling of growth energetics,<sup>41,42</sup> on select low-index orientations may be sufficient to predict growth over most of orientation space. In the standard models of epitaxial energetics,<sup>2</sup> the observation that the eutactic OR is found for all substrate orientations (and subsequent substrate-film interface and film surface planes) implies that either: (i) the interfacial

energies of the eutactic OR are lower than interfacial energies of all other potential ORs, for all substrate orientations, or (ii) the kinetic barriers to formation of critical nuclei are lower for the eutactic OR than for ORs with lower overall interface energies.

In homopolytypic growth, for example,  $3C$  on  $3C$  or  $4H$  on  $4H$ , the eutaxial arrangement is the unit-cell over unit-cell arrangement, which is well known in epitaxial growth of  $3C$  perovskites on single crystals. In prior CSE work, it was shown that  $3C$  BiFeO<sub>3</sub> grew in this fashion on  $3C$  La<sub>0.7</sub>Sr<sub>0.3</sub>MnO<sub>3</sub>-buffered  $3C$  LaAlO<sub>3</sub> substrates,<sup>13</sup> as did  $3C$  Sr<sub>2</sub>FeMoO<sub>6</sub> on  $3C$  Sr<sub>2</sub>MgWO<sub>6</sub>.<sup>15</sup> For the metastable  $3C$  SrMnO<sub>3</sub> investigated herein, this was also observed on (100) oriented SrTiO<sub>3</sub> single crystals, similar to earlier reports,<sup>35,36</sup> and on (100) oriented grains in SrTiO<sub>3</sub> polycrystals. By using  $4H$  SrMnO<sub>3</sub> polycrystalline substrates, we have shown that homoepitaxial growth occurs over all of orientation space and is consistent with the eutaxial OR, or unit-cell over unit-cell OR. For homopolytypic growth, one expects the unit-cell over unit-cell OR to lead to the lowest energy interface, as all bonds can be nominally satisfied across the interface.

For the heteropolytypic epitaxial growth, which includes  $3C$  CaMnO<sub>3</sub> on  $4H$  SrMnO<sub>3</sub> and  $4H$  SrMnO<sub>3</sub> on  $3C$  SrTiO<sub>3</sub>, the eutaxial arrangement is also observed as the PEO across orientation space. Most importantly, this further supports the eutaxial OR as being a general description of epitaxy when the structures of the film and substrate can be described by eutactic packing, regardless of the substrate orientation, consistent with prior CSE observations for films with different structures than the substrates.<sup>8,9,11,12,42</sup> The preference for the eutactic OR likely arises because it leads to the lowest energy interface amongst the myriad of potential ORs. One expects a relatively low energy interface when the eutactic plane is also the interfacial plane, because these can usually be described as coherent interfaces<sup>8,9,11,12,42</sup> whose energies can be computed.<sup>42</sup> The interface energies across the rest of orientation space for the eutactic OR are less obviously considered as low energy, as such interfaces can be (at best) described as semi-coherent (discussed below for a  $4H$ - $3C$  interface and elsewhere for rutile and anatase on  $3C$  perovskites<sup>42</sup>). Nevertheless, the semi-coherent interfaces for the eutactic OR need only have energies that are lower than those for any other potential OR (also likely generating a semi-coherent to incoherent interface) to be consistently observed as the PEO for all orientations, even though their specific interface energies may be significantly higher than that of the coherent eutaxial interface. Further experimental and computational work is needed to support this as a general rule of interfacial energies.

Surprisingly, heteropolytypic growth of perovskites is not discussed much in the literature, in contrast to the wealth of information available for  $3C$  growth on  $3C$  substrates. Epitaxial  $4H$  BaRuO<sub>3</sub> was stabilized on (111) and (100) SrTiO<sub>3</sub> single

crystals.<sup>43-45</sup> The eutaxial OR was reported on the (111) SrTiO<sub>3</sub> single crystal, in agreement with  $4H$  SrMnO<sub>3</sub> deposited on single crystals and polycrystals via CSE herein. The epitaxy of  $4H$  BaRuO<sub>3</sub> on (100) SrTiO<sub>3</sub> was described as  $\{02\bar{2}3\}\langle 2110\rangle_{4H-f}||\{001\}\langle 110\rangle_{3C-s}$ . The in-plane relationship is identical to the eutaxial arrangement, while the out-of-plane relationship leads to a small angular difference (of 2.6°) from the perfect eutaxial angle for SrMnO<sub>3</sub>. There is another high index plane, the  $\{03\bar{3}4\}$ , which is observed herein as the orientation of  $4H$  SrMnO<sub>3</sub> in grains 2 and 3 from Figure 4. This orientation is only 0.6° away from the exact eutaxial angle for SrMnO<sub>3</sub>. The two cases have an angular separation of 3.2° and in general agree with the eutaxial OR as the epitaxy driver, while the exact local plane that satisfies the eutaxial arrangement is the one that best satisfies overall energy minimization. A similar set of arguments can be used to predict the OR on the  $3C$   $\{110\}$  planes, which would be the  $4H$   $\{01\bar{1}3\}$  plane with the eutactic directions aligned. This also has only partial epitaxial matching between the planes (has a semi-coherent interface), and the exact plane observed may vary by a few degrees. The variation across orientation space of the exact angle between the eutactic planes and directions is consistent with some local variation of this sort.

Lee et al.<sup>43,44</sup> pointed to a similarity of local structural motifs between the  $4H$   $\{02\bar{2}3\}$  and the  $3C$   $\{100\}$  planes, specifically the AEO elements, along with a reasonable coherency along the (eutactic) in-plane directions, to rationalize the specific epitaxial OR observed. However, it is difficult to extrapolate that rationalization of an individual result to a larger predictive trend, as the overall structural match is generally quite poor between these two planes. They both consist of stripes less than 1 nm wide of similar bonding along the eutactic directions, but these stripes do not have any short range coherency (eg, <7 nm) in the orthogonal direction. Importantly, the same arguments can be made for the similarity of the  $4H$   $\{03\bar{3}4\}$  with the  $3C$   $\{100\}$  plane. Thus, qualitatively considering the planar arrangements, either interface appears reasonable, and both are semi-coherent to incoherent. Using CSE observations that the PEO is the eutactic OR, one can broadly predict the expected epitaxy across all of orientation space, regardless of the specifics of the local interface. This is further supported by CSE observations that the eutactic OR is observed across all of orientation space for the growth of  $3C$  CaMnO<sub>3</sub> films on  $4H$  SrMnO<sub>3</sub> substrates, which essentially the inverse growth to that described above.

It is always important in CSE, or any high-throughput characterization method, to ensure that automated phase identification is accurate for all phases and orientations. Based on the positive identification of all substrate grains as the expected phase, we are confident that the phase identification process is accurate for bulk materials. However, in film patterns with lower CIs, the accuracy of phase identification becomes questionable using OIM as the patterns

become more diffuse. This issue is primarily relevant for the case of  $3C$  films grains 2 and 3 from Figure 4. Slight rotations away from the  $3C$  (100) substrate appear to cause some Kikuchi bands from the film to disappear, making it difficult for the OIM software to distinguish between possible phases and orientation. An alternative indexing approach, called dictionary indexing (DI), was used to generate orientation and phase maps from the film in Figure 4 (shown in Appendix S5) using a pattern similarity metric (see Appendix S5). In the DI approach, only grain 1 indexed as the  $3C$  polytype, while grains 2 and 3 were  $4H$ . It is conceivable that both  $4H$  and  $3C$  polytypes were grown on the latter grains, but further analysis using transmission electron microscopy may be needed to resolve this issue. The impact on the conclusions herein is minimal, as these grain orientations are near the phase boundary, and one expects possible two phase nucleation events near boundaries.

The limited range of epitaxial stabilization of metastable compounds in the  $AEMnO_3$  family indicates that the penalties of higher interfacial and/or strain energies for heteropolytypic growth of the stable phase are not significant enough to overcome the inherent preference in volumetric formation energy for the stable phase, across most of film-substrate synthesis space. That  $3C$   $CaMnO_3$  epitaxially deposited on a  $4H$   $SrMnO_3$  polycrystalline substrate showed no significant evidence of a new hexagonal phase reinforces this difficulty in stabilizing metastable perovskite polytypes by epitaxy, in these growth conditions. In the conditions used here, the  $4H$  polytype of  $SrMnO_3$  is stable. Only the (100) surface of  $3C$   $SrTiO_3$  substrate inverts the polytype stability during growth of  $SrMnO_3$ . At lower oxygen pressures, one expects growth of oxygen-deficient  $SrMnO_{3-\delta}$  with less hexagonal and more cubic stacking, leading to a transition from  $4H$  to  $3C$  polytype for  $SrMnO_{3-\delta}$  as  $\delta$  increases. Unfortunately, the exact composition of the films are not known in these conditions, nor are the differences in formation energies of the two polytypes of  $SrMnO_{3-\delta}$  and of  $CaMnO_{3-\delta}$ , nor are the interfacial and strain energies for any of the film-substrate pairs investigated. Therefore, high-throughput empirical methods, such as CSE, are needed to drive materials design using epitaxy, particularly by establishing PEOs and epitaxial stability windows.

It has been postulated by Mehta et al.<sup>41</sup> that, given the ideal differences in the interfacial and strain energy terms, metastable phases could be stabilized epitaxially if the volumetric difference  $\lesssim 20$  kJ/mol. Xu et al.<sup>42</sup> showed that computational methods can guide understanding of polymorph competition during growth of anatase and rutile on low index surfaces, especially when the PEO is well established. The relative order of stability computed using density functional theory (DFT) for the two polymorphs across orientation space agreed with both single crystal and CSE experiments. The empirical results here imply that the magnitude of volumetric energy difference that can be overcome is possibly more narrow for these polytypic

structures when growth is driven on the eutactic planes, where the penalty along the eutactic packing direction to form a different polytype is essentially identical to stacking faults, which are known to form in all of the hexagonal polytypes.<sup>30,31,46,47</sup>

Thus, computational estimates of the stacking fault and strain energy penalties for eutactic epitaxy between polytypes could provide important guidance to the level of metastability that can be surmounted in the  $AEMnO_{3-\delta}$  ( $AE = Ca, Sr, \text{ and } Ba$ ) system, especially when linked to composition. On the other hand, the planar lattice matching of the eutaxial ORs along the non-eutactic low-index  $3C$  substrate orientations (such as the {100} and {110}) are similar to the semi- or in-coherent interfaces discussed in Mehta et al.<sup>41</sup> and should be relatively high in energy compared to isostructural interfaces on the same surfaces. In this view, the origin of the limited orientation range of stable  $3C$   $SrMnO_3$  is still in question. To unravel this, both computational and physical experiments are needed to understand the role of synthesis conditions, especially temperature, oxygen pressure, and deposition rate, on phase stability and growth, especially in the  $2H/4H/3C$  competition in the  $AEMnO_3$  systems. It is clear that epitaxial stabilization of distinct polytypes, such as  $3C$   $BaMnO_3$  on  $3C$  perovskite substrates, will require strict control over the chemical, strain, and interfacial energies by appropriate choices of deposition conditions and perhaps novel substrates.

## 5 | CONCLUSIONS

The PEOs were determined using orientation data from EBSD for  $4H$  and  $3C$  perovskite polytypes of  $CaMnO_3$  and  $SrMnO_3$  films, grown on several polycrystalline  $4H$  and  $3C$  substrates via pulsed laser deposition. A single epitaxial OR was found to describe the PEO for all polytypic film-substrate pairs, which we call the eutaxial OR, or the OR that aligns the eutactic planes and direction between their respective crystal structures. This can be written as follows for the specific films explored here:  $(001)[100]_{4H-f} || (001)[100]_{4H-s}; (111)[\bar{1}\bar{1}0]_{3C-f} || (001)[100]_{4H-s}; (001)[100]_{4H-f} || (111)[\bar{1}\bar{1}0]_{3C-s}$ . These were clearly observed over almost all of substrate orientation space for  $4H$   $SrMnO_3$  on polycrystalline  $4H$   $SrMnO_3$  and  $3C$   $SrTiO_3$ , as well as  $3C$   $CaMnO_3$  on polycrystalline  $4H$   $SrMnO_3$ . This prevalence of the eutactic OR can be understood if its interface energies represent the lower bound of interface energies regardless of orientation. Epitaxial stabilization of metastable  $3C$   $SrMnO_3$  was observed only in a very narrow range of orientation space on  $3C$   $SrTiO_3$  substrates: on (100) single crystals and on nearly (100)-oriented surfaces of polycrystals. This narrow range stands in contrast to many other CSE observations, indicating that, in these growth conditions, the energetic penalty of the interface between different polytypes is relatively low, and unable to drive extensive epitaxial stabilization. The absence of

substrate driven metastable  $4H$   $\text{CaMnO}_3$  further supports this conclusion. The combined results, however, support the idea that CSE can quickly unravel the nature of epitaxial growth and competitive polymorph nucleation, and should allow for computational predictions of epitaxial growth.

## ACKNOWLEDGMENTS

CZ, PAS, and GSR acknowledge the support of the National Science Foundation (DMR-1609355). MDG wishes to acknowledge funding from the US Department of Defense Vannevar-Bush Faculty Fellowship (N00014-16-1-2821). The authors also acknowledge the use of the Materials Characterization Facility at Carnegie Mellon University (MCF-677785).

## ORCID

Catherine Zhou  <https://orcid.org/0000-0003-3387-7979>

Gregory S. Rohrer  <https://orcid.org/0000-0002-9671-3034>

[org/0000-0002-9671-3034](https://orcid.org/0000-0002-9671-3034)

Paul A. Salvador  <https://orcid.org/0000-0001-7106-0017>

## REFERENCES

- Martin LW, Chu YH, Ramesh R. Advances in the growth and characterization of magnetic, ferroelectric, and multiferroic oxide thin films. *Mater Sci Eng R Rep*. 2010;68(4–6):89–133.
- Gorbenko OY, Samoilenkov SV, Graboy IE, Kaul AR. Epitaxial stabilization of oxides in thin films. *Chem Mater*. 2002;14(10):4026–43.
- Schlom DG, Chen LQ, Pan X, Schmehl A, Zurbuchen MA. A thin film approach to engineering functionality into oxides. *J Am Ceram Soc*. 2008;91(8):2429–54.
- Mercey B, Salvador PA, Prellier W, Doan T-D, Wolfman J, Hervieu M, et al. Thin film deposition: a novel synthetic route to new materials. *J Mater Chem*. 1999;9(1):233–42.
- Salvador PA, Doan TD, Mercey B, Raveau B. Stabilization of  $\text{YMnO}_3$  in a perovskite structure as a thin film. *Chem Mater*. 1998;10(10):2592–5.
- Moreira dos Santos AF, Cheetham AK, Tian W, Pan X, Jia Y, Murphy NJ, et al. Epitaxial growth and properties of metastable  $\text{BiMnO}_3$  thin films. *Appl Phys Lett*. 2004;84(1):91–3.
- Balasubramaniam KR, Havelia S, Salvador PA, Zheng H, Mitchell JF. Epitaxial stabilization and structural properties of  $\text{REMnO}_3$  (RE=Dy, Gd, Sm) compounds in a layered, hexagonal  $\text{ABO}_3$  structure. *Appl Phys Lett*. 2007;91(23):232901.
- Burbure NV, Salvador PA, Rohrer GS. Orientation and phase relationships between titania films and polycrystalline  $\text{BaTiO}_3$  substrates as determined by electron backscatter diffraction mapping. *J Am Ceram Soc*. 2010;93(9):2530–3.
- Zhang Y, Schultz AM, Li L, Chien H, Salvador PA, Rohrer GS. Combinatorial substrate epitaxy: a high-throughput method for determining phase and orientation relationships and its application to  $\text{BiFeO}_3/\text{TiO}_2$  heterostructures. *Acta Mater*. 2012;60(19):6486–93.
- Havelia S, Wang S, Balasubramaniam KR, Schultz AM, Rohrer GS, Salvador PA. Combinatorial substrate epitaxy: a new approach to growth of complex metastable compounds. *Cryst Eng Comm*. 2013;15(27):5434–41.
- Wittkamper J, Xu Z, Kombaiah B, Ram F, De Graef M, Kitchin JR, et al. Competitive growth of scrutinyite ( $\alpha\text{-PbO}_2$ ) and rutile polymorphs of  $\text{SnO}_2$  on all orientations of columbite  $\text{CoNb}_2\text{O}_6$  substrates. *Cryst Growth Des*. 2017;17(7):3929–39.
- Schultz AM, Zhu Y, Bojarski SA, Rohrer GS, Salvador PA. Eutaxial growth of hematite  $\text{Fe}_2\text{O}_3$  films on perovskite  $\text{SrTiO}_3$  polycrystalline substrates. *Thin Solid Films*. 2013;548:220–4.
- Pravarthana D, Trassin M, Haw Chu J, Lacotte M, David A, Ramesh R, et al.  $\text{BiFeO}_3/\text{La}_{0.7}\text{Sr}_{0.3}\text{MnO}_3$  heterostructures deposited on spark plasma sintered  $\text{LaAlO}_3$  substrates. *Appl Phys Lett*. 2014;104(8):082914.
- Lacotte M, David A, Pravarthana D, Grygiel C, Rohrer GS, Salvador PA, et al. Growth of  $\text{Ca}_2\text{MnO}_4$  Ruddlesden-Popper structured thin films using combinatorial substrate epitaxy. *J Appl Phys*. 2014;116(24):245303.
- Santosh M, Lacotte M, David A, Boullay P, Grygiel C, Pravarthana D, et al. Pulsed laser deposition of  $\text{Sr}_2\text{FeMoO}_6$  thin films grown on spark plasma sintered  $\text{Sr}_2\text{MgWO}_6$  substrates. *J Phys D: Appl Phys*. 2017;50(23):235301.
- Marthinsen A, Faber C, Aschauer U, Spaldin NA, Selbach SM. Coupling and competition between ferroelectricity, magnetism, strain, and oxygen vacancies in  $\text{AMnO}_3$  perovskites. *MRS Commun*. 2016;6(3):182–91.
- Søndenå R, Stølen S, Ravindran P, Grande T, Allan NL. Corner-versus face-sharing octahedra in  $\text{AMnO}_3$  perovskites (A=Ca, Sr, and Ba). *Phys Rev B*. 2007;75(18):184105.
- Søndenå R, Ravindran P, Stølen S, Grande T, Hanfland M. Electronic structure and magnetic properties of cubic and hexagonal  $\text{SrMnO}_3$ . *Phys Rev B*. 2006;74(14):144102.
- Song RN, Hu MH, Chen XR, Guo JD. Epitaxial growth and thermostability of cubic and hexagonal  $\text{SrMnO}_3$  films on  $\text{SrTiO}_3(111)$ . *Front Phys*. 2015;10(3):321–6.
- Belik AA, Matsushita Y, Katsuya Y, Tanaka M, Kolodiaznyhny T, Isobe M, et al. Crystal structure and magnetic properties of  $6H\text{-SrMnO}_3$ . *Phys Rev B*. 2011;84(9):94438.
- Molinari M, Tompsett DA, Parker SC, Azough F, Freer R. Structural, electronic and thermoelectric behaviour of  $\text{CaMnO}_3$  and  $\text{CaMnO}_{(3-8)}$ . *J Mater Chem A*. 2014;2(34):14109–17.
- Adkin JJ, Hayward MA.  $\text{BaMnO}_{3-x}$  revisited: a structural and magnetic study. *Chem Mater*. 2007;19(4):755–62.
- Chamberland BL, Sleight AW, Weiher JF. Preparation and characterization of  $\text{BaMnO}_3$  and  $\text{SrMnO}_3$  polytypes. *J Solid State Chem*. 1970;1(3):506–11.
- Dabrowski B, Chmaissem O, Mais J, Kolesnik S, Jorgensen JD, Short S. Tolerance factor rules for  $\text{Sr}_{1-x}\text{Ca}_x\text{Ba}_y\text{MnO}_3$  perovskites. *J Solid State Chem*. 2003;170(1):154–64.
- Longo JM, Kafalas JA. The effect of pressure and B-cation size on the crystal structure of  $\text{CsBF}_3$  compounds (B=Mn, Fe Co, Ni, Zn, Mg). *J Solid State Chem*. 1969;1(1):103–8.
- Longo JM, Kafalas JA. Pressure-induced structural changes in the system  $\text{Ba}_{1-x}\text{Sr}_x\text{RuO}_3$ . *Mater Res Bull*. 1968;3(8):687–92.
- Goodenough JB. Theory of the role of covalence in the perovskite-type manganites  $[\text{La}, \text{M(II)}]\text{MnO}_3$ . *Phys Rev*. 1955;100(2):564–73.
- Haghir-Gosnet AM, Renard JP. CMR manganites: physics, thin films and devices. *J Phys D: Appl Phys*. 2003;36(8):R127–92.
- Goldschmidt VM. Die Gesetze der Kristallochemie. *Naturwissenschaften*. 1926;14(21):477–85.

30. Negas T, Roth RS. Phase equilibria and structural relations in the system  $\text{BaMnO}_{3-x}$ . *J Solid State Chem.* 1971;3(3):323–39.
31. Negas T, Roth RS. The system  $\text{SrMnO}_{3-x}$ . *J Solid State Chem.* 1970;1(3):409–18.
32. Zhou Q, Kennedy BJ. Thermal expansion and structure of orthorhombic  $\text{CaMnO}_3$ . *J Phys Chem Solids.* 2006;67(7):1595–8.
33. Taguchi H, Nagao M, Sato T, Shimada M. High-temperature phase transition of  $\text{CaMnO}_{3-\delta}$ . *J Solid State Chem.* 1989;78(2):312–5.
34. Rondinelli JM, Eidelson AS, Spaldin NA. Non- $d^0$  Mn-driven ferroelectricity in antiferromagnetic  $\text{BaMnO}_3$ . *Phys Rev B.* 2009;79(20):205119.
35. Francis AJ, Salvador PA. Synthesis structures and physical properties of yttrium-doped strontium manganese oxide films. *MRS Online Proceedings.* 2002;718:D9.4.
36. Kobayashi S, Tokuda Y, Ohnishi T, Mizoguchi T, Shibata N, Sato Y, et al. Cation off-stoichiometric  $\text{SrMnO}_{3-\delta}$  thin film grown by pulsed laser deposition. *J Mater Sci.* 2011;46(12):4354–60.
37. Maurel L, Marciano N, Prokscha T, Langenberg E, Blasco J, Guzm'an R, et al. Nature of antiferromagnetic order in epitaxially strained multiferroic  $\text{SrMnO}_3$  thin films. *Phys Rev B.* 2015;92(2):24419.
38. Nielsen MB, Ceresoli D, Parisiades P, Prakapenka VB, Yu T, Wang Y, et al. Phase stability of the  $\text{SrMnO}_3$  hexagonal perovskite system at high pressure and temperature. *Phys Rev B.* 2014;90(21):214101.
39. Ohring M. *Materials Science of Thin Films.* San Diego, CA: Academic Press; 2002.
40. Zhang J, Tanaka H, Kanki T, Choi JH, Kawai T. Strain effect and the phase diagram of  $\text{La}_{1-x}\text{Ba}_x\text{MnO}_3$  thin films. *Phys Rev B.* 2001;64(18):184404.
41. Mehta P, Salvador PA, Kitchin JR. Identifying potential  $\text{BO}_2$  oxide polymorphs for epitaxial growth candidates. *ACS Appl Mater Interfaces.* 2014;6(5):3630–9.
42. Xu Z, Salvador PA, Kitchin JR. First-principles investigation of the epitaxial stabilization of oxide polymorphs:  $\text{TiO}_2$  on  $(\text{Sr}, \text{Ba})\text{TiO}_3$ . *ACS Appl Mater Interfaces.* 2017;9(4):4106–18.
43. Lee MK, Eom CB, Tian W, Pan XQ, Smoak MC, Tsui F, et al. Synthesis and properties of epitaxial thin films of c-axis oriented metastable four-layered hexagonal  $\text{BaRuO}_3$ . *Appl Phys Lett.* 2000;77(3):364–6.
44. Lee MK, Eom CB, Lettieri J, Scrymgeour IW, Schlom DG, Tian W, et al. Epitaxial thin films of hexagonal  $\text{BaRuO}_3$  on (001)  $\text{SrTiO}_3$ . *Appl Phys Lett.* 2001;78(3):329–31.
45. Tian W, Pan XQ, Lee MK, Eom CB. Microstructure of  $\text{BaRuO}_3$  thin films grown on (001)  $\text{SrTiO}_3$ . *Appl Phys Lett.* 2000;77(13):1985–7.
46. Parras M, Alonso J, Gonz'alez-Calbet JM, Vallet-Reg'i M. Ordering and defects in  $\text{BaMnO}_{3-y}$  ( $0.22 \leq y \leq 0.40$ ). *J Solid State Chem.* 1995;117(1):21–9.
47. Shibahara H. Electron microscope study of the structure of  $\text{SrMnO}_{3-x}$  with planar defect. *J Mater Res.* 1991;6(3):565–73.

## SUPPORTING INFORMATION

Additional supporting information may be found online in the Supporting Information section.

**How to cite this article:** Zhou C, De Graef M, Dabrowski B, Rohrer GS, Salvador PA. Combinatorial substrate epitaxy investigation of polytypic growth of  $\text{AEMnO}_3$  ( $\text{AE} = \text{Ca}, \text{Sr}$ ). *J Am Ceram Soc.* 2020;103:2225–2234. <https://doi.org/10.1111/jace.16867>